RSC Advances

ROYAL SOCIETY OF CHEMISTRY

www.rsc.org/advances

Graphical Abstract

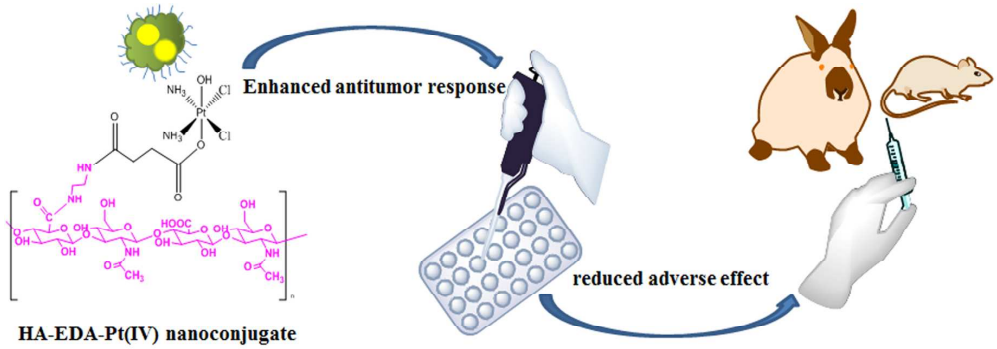

HA-EDA-Pt(IV) nanoconjugates were constructed, characterized, and proved as an safe formulation with better blood compatibility and less systemic toxicity.

Synthesis and characterization of hyaluronic acid-platinum(IV) nanoconjugate with enhanced antitumor response and reduced adverse effect

Xiang Ling [a], Chunyang Zhao [b], Liping Huang [a], Qiyue Wang [a], Jiasheng Tu [a, *], Yan Shen [a], Chunmeng Sun [a, *]

[a] State Key Laboratory of Natural Medicines, Department of Pharmaceutics, School of Pharmacy, China Pharmaceutical University, Nanjing 210009, China

[b] State Key Laboratory of Bioactive Substances and Functions of Natural Medicines, Institute of Materia Medica, Chinese Academy of Medical Sciences & Peking Union Medical College, Beijing 100050, China

* Corresponding authors. Address: 24 Tong Jia Xiang, Nanjing 210009, China. Tel.: +86-25-83271305. Fax: +86-25-83301606. E-mail: suncm_cpu@hotmail.com (C. Sun); jiashengtu@aliyun.com (J. Tu).

Abstract

Hyaluronic acid-platinum(IV) nanoconjugate with a high drug loading capacity was developed to mitigate side effects of platinum(II). Pt(IV), HA-EDA, and HA-EDA-Pt(IV) nanoconjugate were investigated by ^{1}H NMR, ^{13}C NMR, FT-NIR, and DSC. Negatively charged polymer-drug conjugates were of a uniform size around 186.4 nm and spherical in shape. *In vitro* antiproliferation and *in vivo* apoptosis assays proved that the nanomedicine possessed high cytotoxicity towards cancer cells. The enhanced antitumor effect was attributed to HA receptor-mediated endocytosis. Nanoscale conjugates exhibited desirable blood compatibility and negligible stimulation to blood vessels. The systemic toxicity study showed that polymer-drug conjugates were much safer than the parent drug evidenced by biochemical and histological analyses. The concise design of the nanoconjugate offers a simple way to overcome the toxicity and non-selectivity of cisplatin, which could improve therapeutical outcomes of platinum drugs in cancer therapy.

Keywords: hyaluronic acid; platinum(IV); nanoconjugate; cisplatin; toxicity;

1. Introduction

Adverse reactions have been frequently reported for anti-cancer drugs because of their off-target exposure to normal cells. It has been demonstrated nanomaterials carrying therapeutic and diagnostic agent could enable selective accumulation in diseased tissues, efficient internalization by targeted cells, and effective intracellular trafficking [1-5]. Therefore, there is a great interest in the development of drug delivery systems that could improve the pharmacokinetic profiles and ultimately the therapeutic outcomes of anti-cancer drugs [6-13]. In 1965, it was first reported that platinum compounds could inhibit cell division [14]. Among those compounds, the most potent one is cisplatin with a broad-spectrum antitumor effect. Nevertheless, frequently occurring adverse reactions, such as nephrotoxicity, peripheral neuropathy, and hearing loss, encumber cisplatin from wide clinical applications [15]. To overcome those deficiencies, much attention has been paid to inert Pt(IV) counterparts, which could be released and reduced to active Pt(II) counterparts in cancer cells under an mildly acid microenvironment with high levels of reductive substances, e.g., glutathione, ascorbic acid, cysteine, and metallothioneins [16-19]. Owning to desirable stability in blood circulation and fast reduction from + IV to + II valence inside targeted cells, platinum-based pro-drugs may act as first-line antitumor agents [20].

Polymer-drug conjugates can preferentially accumulate in tumor tissues due to the Enhanced Permeability and Retention (EPR) effect [21]. An acid-sensitive pro-drug conjugate was designed via linking two hydrophobic ends of PEG-PLA with a Pt(IV) counterpart as a spacer, subsequently forming nanoparticles to achieve stronger cytotoxicity as compared to cisplatin [22]. However, considering lack of specificity of most reported carriers taken up via non-receptor-mediated bulk endocytosis, further studies were concentrated on conferring Pt(IV) delivery systems with

targeting competence to promote endocytosis [23]. One of the most promising scenarios is applying hyaluronic acid (HA) as the carrier of cargos on the basis of over-expressed HA receptors, i.e., CD44, RHAMM, HARE, LYVE-1, on the surface of most malignant cells [24, 25]. Our group utilized HA, both as a biodegradable skeleton and a specific tumor hunter for targeted delivery of cisplatin(IV). Previously we had reported HA-EDA-Pt(IV) nanoconjugate could enhance the anti-tumor efficacy yet reduce the toxicity of cisplatin [26]. However, the physiochemical properties and biocompatibility of our nanoconjugate were not scrutinized, which would be essential towards developing a clinically meaningful formulation. Therefore, the present study aimed at further understanding the *in vitro* and *in vivo* properties of the nanomedicine.

As illustrated in Fig. 1, cisplatin was oxidized with H_2O_2 and esterified with succinic anhydride to obtain cis,cis,trans-dichoro-hydroxyl-succinato-platinum(IV), abbreviated as Pt(IV). Meanwhile, HA was modified with ethylenediamine to form HA-EDA with NH_2-functionalized pendants. Finally, HA-EDA-Pt(IV) nanoconjugate was yielded via succinate amide bonds between Pt(IV) and HA-EDA with an adjustable platinum content. Several physicochemical properties of the nanoconjugate were investigated. Studies on antiproliferation, cellular uptake, apoptosis as well as safety evaluation were also conducted.

2. Materials and methods

2.1. Materials

Hyaluronic acid (11 kDa) was supplied by Freda Biochem. Cisplatin was obtained from Boyuan Pharmaceutical Chemical Company. Ethylenediamine dihydrochloride (EDA·2HCl), succinic anhydride, 3-(4,5-dimethylthiazol-2-yl)-2,5-diphenyltetrazolium bromide (MTT) and

4,6-diamidino-2-phenylindole dihydrochloride (DAPI) were provided by Sigma-Aldrich. R isomer [Tetramethylrhodamine-6-isothiocyanate] (TRITC) was bought from Fanbo Biochemicals. N-(3-Dimethylaminopropyl)-N'-ethylcarbodiimide hydrochloride (EDC·HCl), N-Hydroxysuccinimide (NHS) and 2,4,6-trinitrobenzenesulfonic acid solution (TNBS) were offered by Aladdin. Annexin V-FITC/PI apoptosis detection kit was purchased from BD Biosciences. Dulbecco's Modified Eagle's Medium (DMEM) and Minimum Essential Medium (MEM), trypsin, fetal bovine serum (FBS), penicillin-streptomycin solution, phosphate buffered saline (PBS) were presented by Gibco®.

2.2. Cell culture and animal use

B16-F10 and Hep G2 obtained from Cell Bank of Shanghai Institute of Biochemistry and Cell Biology, Chinese Academy of Sciences was grown in DMEM and MEM, respectively, supplemented with 10 v/v% FBS, 100 U/mL penicillin and streptomycin. Exponentially growing cultures were maintained at 37 ℃ under an atmosphere of 5% CO_2 and 90% relative humidity.

New Zealand rabbits were purchased from Laboratory Animal Research Center of Jiangsu University. C57BL/6J mice were obtained from SLRC Laboratory Animal Center. ICR mice were bought from College of Veterinary Medicine Yangzhou University. They were kept at 22 ± 2 ℃ and 70 ± 5% relative humidity under natural light-dark conditions with free access to food and water. All care and handling of animals were conducted in accordance with the National Institute of Health Guide for the Care and Use of Laboratory Animals and approved by the Animal Ethics Committee of China Pharmaceutical University.

2.3. Preparation of HA-EDA-Pt(IV) nanoconjugate

2.3.1. Synthesis of cis,cis,trans-[$Pt(NH_3)_2Cl_2(OH)_2$]

30 w/v% H_2O_2 (4.0 mL) was added into 10% cisplatin suspension (10.0 mL) and the mixture was kept stirring against light at 25 ℃ for 24 h. After recrystallization at 4 ℃, the product was collected and washed with ice cold water, ethanol and diethyl ether. Then residual solvent was removed to give bright yellow powder (yield: 90.3%) [27].

2.3.2. Synthesis of cis,cis,trans-[$Pt(NH_3)_2Cl_2(OOCCH_2CH_2COOH)(OH)$]

Equimolar amounts (0.60 mmol) of cis,cis,trans-[$Pt(NH_3)_2Cl_2(OH)_2$] and succinic anhydride dissolved in 16.0 mL dimethyl sulfoxide (DMSO) were kept stirring in the dark at 25 ℃ for 12 h. After lyophilization, Pt(IV), as yellow needle crystals, was afforded by recrystallization from acetone (-20 ℃), washed with cold acetone and diethyl ether (yield: 65.2%) [28].

2.3.3. Synthesis of ethylenediamine modified hyaluronic acid

EDC·HCl (0.12 g) was added into 2% HA solution in PBS (10.0 mL, pH 7.4, 10 mM). 15 min later, EDA·2HCl (2.66 g) in same volume PBS was added dropwise. The mixture was adjusted to neutral pH and allowed to proceed for 2 h at 25 ℃. After exhaustive dialysis (MWCO, 3.5 kDa) against 100 mM NaCl and deionized water, the solution was filtered through a 0.22 μm retention size filter, lyophilized and stored at 4 ℃ [29].

2.3.4. Conjugate cis,cis,trans-[$Pt(NH_3)_2Cl_2(OOCCH_2CH_2COOH)(OH)$] to HA-EDA

EDC·HCl (0.19 g), NHS (0.12 g) and Pt(IV) (0.35 g) were dissolved in PBS (pH 6.5, 10 mM,

6.0 mL) and kept from light under ice bath stirring. 0.5% HA-EDA solution in PBS (20.0 mL) was added, stirred for 24 h, dialyzed (MWCO 3.5 kDa) against deionized water and lyophilized. The drug loading capacity of platinum was calculated:

$$\text{Drug loading capacity (\%)} = \frac{\text{Weight of charged platinum}}{\text{Weight of the nanoconjugate}} \times 100$$

2.3.5. Synthesis of HA-EDA-Pt(IV)-TRITC

3% Polymer-drug conjugates in 3.0 mL carbonate buffer solution and 0.1% TRITC in 1.0 mL DMSO, avoiding light, were kept stirring for 24 h, dialyzed (MWCO 3.5 kDa), and lyophilized. The loading capacity was determined by Fluorescence Spectrophotometer (Lumina, Thermo Fisher Scientific, USA).

2.3.6. General measurements

^{1}H NMR and ^{13}C NMR spectra were recorded on Bruker AV-500 and AV-300 (Switzerland), respectively. Fourier Transform Near Infrared (FT-NIR) spectra were conducted on Bruker TENSOR 27 Spectrometer (Germany) using KBr method. Thermal behaviors were analyzed by Differential Scanning Calorimeter (DSC204, NETZSCH Group, Germany): temperature ranged 4~300 ℃ and heating rate was 10.0 K/min. Platinum measurement was operated on iCE 3300 Graphite Furnace Atomic Absorption Spectrometry (GFAAS, Thermo Scientific, USA) with Quadline® deuterium background correction. A platinum hollow cathode lamp with current of 10.0 mA was used as the radiation source at 265.9 nm with a slit width of 0.2 nm. The flow rate of high purity argon was 0.3 L·min^{-1} and stopped during atomizing stage.

2.4. Substitution of ethylenediamine

1.0 mL of solution containing 0.5 w/v% TNBS and 4 w/v% $NaHCO_3$ was added to HA-EDA (2.00 mg) incubated in 1 w/v% trichloroacetic acid (0.2 mL). The reaction was conducted against light for 1 h at 50 ℃. After addition of HCl (3.0 mL, 6 M), temperature was raised to 60 ℃, then cooled and diluted with deionized water. A blank was prepared, except HCl was added before TNBS. The absorbance at 410 nm was assayed via UV-Vis Spectrophotometer (UV-3200, Mapada, China) and correlated according to a calibration curve obtained with valine [30]. The degree of substitution was calculated:

$$\text{Degree of substitution (mol/g)} = \frac{\text{The mole number of primary amine groups}}{\text{The weight of sample}} \times 100$$

2.5. Particle size, zeta potential and morphology

HA-EDA-Pt(IV) nanoconjugate dissolved in physiological saline was measured by Particle Size & Zeta Potential Analyzer (90Plus Zeta, Brookhaven Instruments Corporation, USA).

An aqueous solution of the nanomedicine was dropped on a clean mica surface, dried and visualized by Atomic Force Microscopy (AFM, Nano Scope IIIa, Veeco Instruments, USA) [31].

2.6. *In vitro* cytotoxicity

B16-F10 and Hep G2 (3×10^3 cells/well) were incubated in 96-well plates for 24 h, then mixed with fresh medium containing different formulations. The amounts of HA and HA-EDA were equal to those in the corresponding HA-EDA-Pt(IV) nanoconjugate samples. 24 and 48 h later, 20 μL MTT (5 mg/mL) was added. After 4 h, the medium was removed, 150 mL DMSO was added. The absorbance was measured at 570 nm by

Absorbance Microplate Reader (ELx800, BioTek Instruments, USA).

2.7. Cellular uptake

B16-F10 and Hep G2 (5×10^5 cells/well) were seeded in 6-well plates for 24 h, then exposed to TRITC-labeled nanoconjugate (final TRITC concentration 5, 50 mg/L). At selected time intervals, cells were washed with 4 ℃ PBS, fixed with 4% paraformaldehyde for 20 min, stained with DAPI for 30 s and captured by Inverted Fluorescence Microscope (IFM, Eclipse Ti-SR, Nikon Corporation, Japan). In competition study, HA (200 mg/mL) was pre-incubated with cells for 2 h.

2.8. Apoptosis of cancer cells

The mouse melanoma model was generated by subcutaneously injecting B16-F10 suspension (2×10^5 cells in 0.1 mL PBS) into the right medial lower extremity of C57BL/6J mice (4-5 weeks old, half male and half female). As tumors reached approximately 50 mm^3 in volume, 24 mice were randomly assigned to 4 groups, intravenously injected with different formulations four times at two-day intervals, then euthanized.

Protein extracts from tumors were obtained with a Whole Cell Lysis kit (KGP2100, KeyGEN, China), quantified by BCA protein assay (KGP902, KeyGEN, China) and adjusted to equal concentration. Samples (70 μg/lane) were separated by SDS-PAGE followed by transferring proteins onto a PVDF membrane (BioRad, USA). The membrane was blocked with 5% nonfat dry milk in PBST for 1 h and incubated with primary antibodies (Caspase 3,

Poly(ADP-ribose) polymerase (PARP), Phospho-p53 and β-actin antibodies) at 4 ℃ overnight. Then the membrane was incubated with a HRP conjugated secondary antibody (Jackson ImmunoResearch, USA) for 1 h at room temperature and washed with PBST five times for 5 min. The blots were visualized with ECL detection reagents and exposed on blue autoradiography film (Amersham Biosciences, USA).

2.9. Red blood cells (RBCs) hemolysis

RBCs, collected from rabbit blood, were diluted with physiological saline to 2 v/v%. Samples were dissolved in RBCs suspensions at gradient concentrations, incubated at 37 ℃ for 3 h, centrifuged at 1500 rpm for 15 min. Supernatant was measured via Absorbance Microplate Reader at 541 nm, hemolysis rate was determined:

$$\text{Hemolysis rate (\%)} = \frac{A_{sample} - A_0}{A_{100} - A_0} \times 100$$

Where A_{sample} was the absorbance of sample, A_{100} was the absorbance of lysed RBCs in deionized water (positive control), A_0 was the absorbance of 0% hemolysis in physiological saline (negative control) [32].

2.10. Injection irritation

12 New Zealand rabbits (1.8-2 kg) were randomly divided into 4 groups. Cisplatin and HA-EDA-Pt(IV) nanoconjugate (calculated by cisplatin) made at a rate of 1 mL/min were injected at a dose of 2 mg/kg via left marginal ear vein for three consecutive days. Same volumes of HA-EDA and physiological saline were given to other two groups. Any paradoxical reactions were recorded by an experienced unbiased observer. Injection sites and proximal region were stained

with hematoxylin and eosin (HE), followed by histopathological examination using an Upright Metallurgical Microscope (BX45-DP72, Olympus Corporation, Japan).

2.11. Systemic toxicity

30 ICR mice (20-22 g) were randomly assigned to 3 groups and administrated intravenously three times at a two-day interval as follows: cisplatin (5 mg/kg); HA-EDA-Pt(IV) nanoconjugate (equivalent doses of cisplatin); physiological saline. Blood was collected and centrifuged to obtain plasma for measuring alanine aminotransferase (ALT), aspartate aminotransferase (AST), alkaline phosphatase (ALP), blood urea nitrogen (BUN), serum creatinine (Scr) by Automatic Biochemical Analyzer (UniCel DxC 800 Synchron Clinical System, Beckman Coulter, USA). Heart, liver, spleen, lung, kidney and brain were stained with HE to assess histological alteration via Upright Metallurgical Microscope.

2.12. Statistical analysis

Data were expressed as mean ± SD with at least three times replications. Unpaired student's *t*-test was used for comparison between two-group, one-way analysis of variance (ANOVA) with LSD and S-N-K tests for multiple-group. Asterisk represented statistically significant differences (*, $p < 0.05$; **, $p < 0.01$; ***, $p < 0.001$).

3. Results and discussion

3.1. Analysis of ^{1}H NMR spectra

The peak assignment of cis,cis,trans-[$Pt(NH_3)_2Cl_2(OH)_2$] and Pt(IV) in ^{1}H NMR spectra was

accomplished as reported [18]. Esterification of cis,cis,trans-[$Pt(NH_3)_2Cl_2(OH)_2$] (Fig. 2(A)) with succinic anhydride led to a shift of the peak of NH_3 from 5.50 to 5.96 ppm, meanwhile, new chemical shifts between 2.35-2.41 ppm were assigned to methylene protons of succinic anhydride, verifying the structure of Pt(IV) (Fig. 2(B)). The methyl resonance (δ = 2.03 ppm) of acetamido moiety on HA (Fig.2(C)) was used as an internal standard and new chemical shifts at 2.92 and 3.35 ppm were given by CH_2 of ethylenediamine residue on HA-EDA in Fig. 2(D). Small peaks from 2.36 to 2.68 ppm, assigned to methylene protons from Pt(IV) units, confirmed the successful conjugation of Pt(IV) to HA-EDA and the correct molecular structure of the expected product, HA-EDA-Pt(IV) nanoconjugate (Fig. 2(E)). During the conjugation of Pt(IV) to HA-EDA, NH_2 groups of HA-EDA continued to couple with COOH groups of HA in the present of EDC, which caused crosslinking between macromolecular chains or/and self-crosslinking of single macromolecular chain. It complicated the spectrum of the nanoconjugate, such as multiple peaks (3.00-3.30 ppm) and a stronger peak (2.85 ppm) of methylene protons ('f', 'g'), two new peaks at 1.85 and 1.05 ppm. On the other side, the crosslinked copolymer with increased molecular weight and non-linear structure might be beneficial to reduce renal excretion and improve bioavailability.

3.2. Analysis of ^{13}C NMR spectra

There was no signal observed from cisplatin and cis,cis,trans-[$Pt(NH_3)_2Cl_2(OH)_2$] due to the absence of carbon atom in their chemical constitutions. 'a' and 'b' displayed at 179.77 and 174.17 ppm in Fig. 3(A) were considered as characteristic peaks of carbonyl carbons in Pt(IV). Notably, a small shift of 'a' versus 'b' to a higher field reflected the incorporation of succinic acid to cis,cis,trans-[$Pt(NH_3)_2Cl_2(OH)_2$] via a ester bond. Similarly, 'c' (31.22 ppm) was slightly higher

than ‘d’ (30.22 ppm), which were both methylene carbons. In the ^{13}C NMR spectrum of HA (Fig. 3(B)), peaks at 177.57, 176.8, 63.27, 25.22 ppm belonged to carbonyl (e) and methylic (h) carbons of acetamido, as well as carbon atoms in methylene (g) and carboxyl (f). After grafting with EDA, the characteristic peaks of methylene carbons, ‘i’ and ‘j’, of ethylenediamine in HA-EDA spectrum (Fig. 3(C)) appeared at 45.45 and 39.23 ppm. Afterwards, ‘k’, ‘l’, ‘m+n’ (181.38, 163.16, 37.54 ppm) with tiny shifts which were recognized as the characteristic peaks of carbonyl and methylene carbons from Pt(IV), could be observed again in Fig. 3(D), demonstrating the successful conjugation of Pt(IV) to HA-EDA. The crosslinking reaction also increased carbon atoms in the same chemical environment, and their signals were greatly enhanced, such as ‘i’ at 45.25 ppm, ‘j’ at 57.84 ppm.

3.3. Illustration for FT-NIR spectra

FT-NIR spectra of cisplatin, cis,cis,trans-$[Pt(NH_3)_2Cl_2(OH)_2]$, Pt(IV), HA, HA-EDA and HA-EDA-Pt(IV) nanoconjugate were collected. Cisplatin (Fig. 4(A)) had five characteristic peaks of NH_3 at 3284.2, 3205.0, 1316.0, 1298.1, and 797.9 cm^{-1}, which were attributed to symmetrical and asymmetrical stretching vibration (ν_{N-H}), symmetrical and asymmetrical deformation vibration (δ_{N-H}), out-of-plane bending vibration (γ_{N-H}), respectively. In Fig. 4(B), cis,cis,trans-$[Pt(NH_3)_2Cl_2(OH)_2]$, which was obtained by oxidation of cisplatin, exhibited a sharp and intense OH stretch at 3515.0 cm^{-1}, a strong Pt-OH bend at 1038.1 cm^{-1} and a new Pt-OH stretch at 555.8 cm^{-1}. As shown in Fig 4(C), both the 3512.6 cm^{-1} and 567.4 cm^{-1} bands were weakened owing to the consumption of OH during esterification to produce Pt(IV), and there appeared two characteristic peaks, i.e., 1639.7 and 1695.4 cm^{-1}, belonging to coordinated and free

carboxyl groups, respectively [33]. HA was a naturally linear polysaccharide with plentiful OH and NH groups which contributed to the observed absorption at 3395.4 cm^{-1} in Fig. 4(D), and another characteristic peak belonged to asymmetric carbonyl stretching vibration at 1617.1 cm^{-1}. The spectrum of HA-EDA (Fig. 4(E)) was almost the same to that of HA, however, the characteristic absorption of HA at 1617.1 cm^{-1} existed a slightly offset to 1639.2 cm^{-1}, suggesting the formation of new chemical bonds. After conjugation with pro-drugs, a new peak at 524.4 cm^{-1} was assigned to Pt-OH stretch from pendent Pt(IV) of the nanomedicine (Fig. 4(F)). Importantly, the appearance of resonance at 1643.9 cm^{-1}, which was in good agreement with the peak of pro-drugs, was attributable to coordinated carboxyl group, while the peak of free carboxyl group at 1695.4 cm^{-1} in Pt(IV) disappeared.

3.4. Thermal analysis

To further substantiate successful synthesis of HA-EDA-Pt(IV) nanoconjugate, DSC, one of the most useful tools to distinguish synthetic copolymer and physical mixture, was conducted. Interactions in DSC arrive at a conclusion by elimination of endothermic peaks, appearance of new peaks, variations in peak shape and its onset, peak temperature or melting point and relative peak area or enthalpy [34]. From Fig. 5(A), HA degradation gave two peaks: the endothermic peak at around 86 ℃, suggesting a dehydration process; an exothermic peak at 248 ℃, representing decomposition and resulting in a carbonized residue. In Fig. 5(B), EDA·2HCl had a melting point higher than 300 ℃ [35], which consisted of two maximums with onsets at 129 and 137 ℃, also revealed one complicated thermal anomaly at 134 ℃. The shapes of observed peaks were identical with that reported by Bujak et al and deemed to be typical of a first order phase transition

of the order-disorder type. Nevertheless, the reason why there were two maximums was still unclear and required further study [36]. Calorimetric curve of Pt(IV) (Fig. 5(C)) exhibited a sharp endothermic peak at 169 ℃ and two mild exothermic peaks at 224 and 256 ℃. The former one was the melting point of Pt(IV) and the latter two were resulted from degradation by heat. The physical mixture (Fig. 5(D)) showed most of the characteristic peaks of each component with slight shifts. Unlike the physical mixture, HA-EDA-Pt(IV) nanoconjugate revealed a strikingly contrasting DSC thermogram in Fig. 5(E), where no obvious melting peak of Pt(IV) appeared, indicating that an intact new compound was yielded after multi-step synthesis.

3.5. Estimation of active amine groups and drug loading capacity

As the crosslinking or/and self-crosslinking reaction prevented us from calculating modified units per HA backbone, micromole of active amine groups per milligram of HA-EDA was used to estimate substitution of ethylenediamine. 2,4,6-trinitrobenzenesulfonic acid (TNBS), a colorimetric reagent, primarily neutralizes the amino group to form a soluble complex which renders characteristic absorption. After incubating HA-EDA with TNBS, the absorption at 410 nm was employed to calculate the amount of exposed active amine groups. Concentrations were determined using a standard curve (range: 0.4 to 2.0 μmol/mL) reflecting a linear function: $y = 0.2273x + 0.0007$ ($R^2 = 0.9996$). Ethylenediamine with a shorter alkyl chain might slightly accrete stereo-specific blockade, thereby inducing the degree of modification slightly higher. Batch-to-batch variations of ethylenediamine substitution could be minimized by strictly controlling the ratio of reactants and reaction time, and the amount of active amine groups were consistent at a level of 15-18 μmol/mg. However, the data were different from that calculated

according to ^{1}H NMR. One possible explanation was that active amine groups buried in the core of chemically crosslinked polymers may be inaccessible to TNBS..

Unlike cisplatin, Pt(IV) could readily react with HA-EDA via amidation when catalyzed by EDC/NHS. The platinum content was determined by Graphite Furnace Atomic Absorption Spectrometry (GFAAS) and fixed at 14.84 w/w%. In addition, varying the initial molar feed ratios of Pt(IV) to HA-EDA yielded HA-EDA-Pt(IV) nanoconjugate with various platinum contents, indicating that drug loading capacity could be adjusted conveniently (Data not shown). For cell study, TRITC, a sensitive fluorescent probe, continued to consume residual amino groups of HA-EDA-Pt(IV) nanoconjugate. Finally, TRITC-labeled nanoconjugate was at a modification ratio of 1.03 w/w%. This ratio provided sufficient fluorescent intensity for imaging yet it would minimally affect the intracellular trafficking of our nanomedicine.

3.6. Particle size, zeta potential and morphology of nanoconjugate

As shown in Fig. 6(A, B), HA-EDA presented a unimodal size distribution. After being conjugated with Pt(IV), the unimodal size distribution was sustained and the mean diameter increased from 177.0 ± 2.1 to 186.4 ± 1.3 nm, possibly due to the incorporation of Pt(IV) moieties. In addition, the zeta potential decreased from -25.84 ± 0.73 mV, for HA-EDA, to -28.65 ± 2.01 mV, for HA-EDA-Pt(IV) nanoconjugate, suggesting that Pt(IV) consumed and neutralized some positively charged amino groups in HA-EDA.

In Fig. 6(C, D), all microspheres displayed a spherical morphology with an average diameter of ~ 200 nm, which was larger than that from dynamic light scattering. In addition, the height measured from AFM images was much lower than expected. The increased particle size and

decreased height might result from the spreading or flattening of polymers onto the mica surface during pretreatment.

Taken together, the 200 nm diameter and negative charge would make the nanoconjugate suitable as a novel drug delivery system to achieve accumulation in tumors via EPR effect [37].

3.7. Antiproliferation *in vitro*

B16-F10 and Hep G2 were exposed to platinum drugs at different doses (10, 50, 100, 200, 400 mg/L). HA and HA-EDA were also examined to evaluate their biocompatibility. The relative cell viability-concentration curves were shown in Fig. 7(1). Negligible toxicity to mammalian cells was observed for HA and HA-EDA across the whole tested concentrations. Cisplatin has been widely recognized to have a profound effect on suppressing tumor cell proliferation. As the concentration increased, HA-EDA-Pt(IV) nanoconjugate displayed a comparable or even higher cytotoxicity than cisplatin. Furthermore, prolonging incubation time also led to increased antiproliferative effect. Thus, according to MTT test, it could be concluded that the cytotoxicity of HA-EDA-Pt(IV) nanoconjugate was not impaired upon oxidation and conjugation reaction, and was on a par with that of free cisplatin.

3.8. Cellular internalization

Cellular uptake was carried out on B16-F10 and Hep G2. Apparently, increasing the concentration of HA-EDA-Pt(IV)-TRITC, i.e., from 5 to 50 mg/L, and prolonging the incubation time, i.e., from 4 h to 24 h, resulted in higher internalization, indicating concentration- and time-dependent endocytosis. Importantly, preincubation with free HA greatly inhibited cellular

uptake of HA-EDA-Pt(IV)-TRITC, reflecting that HA receptors played a crucial role in the polymer-drug conjugates transport.

3.9. Activation of *in vivo* apoptosis

To identify cell signaling pathways of *in vivo* apoptosis, western blot was performed. As a family of cysteine proteases, Caspases (cysteine-aspartic proteases) play a prominent role in apoptosis, necrosis, and inflammation [38]. Usually the effector caspases, e.g., Caspase 3, 6, 7, are inactive inside cells till activated by the initiator caspases, e.g., Caspase 2, 8, 9, 10, 11, 12, while different pathways including cellular stress, chemotherapy, radiotherapy, are involved [39]. As shown in Fig. 8A and 8D, band intensity of lane b and d doubled as compared with lane a and c, indicating a dramatically rise of Caspases. Thus significant up-regulation of Caspases 3 was proved in tumor-bearing mice treated with platinum drugs.

PARP is the substrate of Caspases. The activated effector caspases are responsible for cleaved PARP (89 KDa), which is extremely related with a number of cellular processes (mainly DNA repair and apoptosis) [40]. Obviously, treatment with platinum drugs significantly increased cleaved PARP levels of cisplatin versus control groups. However, those tumor-bearing mice treated with HA-EDA-Pt(IV) nanoconjugate resulted in the highest cleaved PARP level (Fig. 8B and 8D). Since the activation of PARP is the last step in triggering apoptosis, it could be concluded that HA-EDA-Pt(IV) nanoconjugate might exert more *in vivo* cytotoxicity to cancer cells than cisplatin.

p53, a tumor suppressor protein that facilitates DNA repair before DNA replication, is considered as a “guardian of the genome” for its activation of a host of other genes that lead to cell

cycle arrest and DNA repair, therefore plays a central role in chemotherapy-induced apoptosis [41]. As expected, HA-EDA-Pt(IV) nanoconjugate group showed the strongest hosphor-p53 signal rather than the physiological saline, cisplatin and HA-EDA groups, thereby indicating the severest apoptosis (Fig. 8C and 8D).

The results obtained from western blot were a full complement of *in vitro* antiproliferation.

3.10. Hemocompatibility

Blood compatibility is considered as one of the most important issues for *in vivo* application of polymer-drug conjugates. The hemolysis ratios were quantified based on spectrophotometric measurements of hemoglobin released from RBCs. When RBCs suspensions were treated with HA, HA-EDA or polymer-drug conjugates, all hemolysis ratios were lower than 1% across the whole tested concentration range, indicating desirable hemocompatibility. In constrast, RBCs exposed to Tween 80 (100 mg/mL) had significant leakage of hemoglobin. And it was found that Tween 80 induced severe hemolysis in a concentration-dependent manner, while other polymers consistently guaranteed much better hemocompatibility.

3.11. Rabbit ear vein irritation test

The visual examination of rabbit ear veins was executed after each administration by a designated bystander. Severe venous irritation was recorded in cisplatin group since the second injection, including vascular engorgement, dropsy, discoloration and induration. In contrast, slight venous irritation was noted in HA-EDA-Pt(IV) nanoconjugate group and no obviously visible damages were found in other groups. Subsequently, rabbit ears were sectioned and stained with

HE. Fig. 9(2) showed microscopic examination of marginal ear veins after injection with sample solutions. In cisplatin group, severe injection irritation such as anapetia, thrombosis, collagen proliferation, and infiltration of inflammatory cells was captured in most regions, even in regions distant from injection sites, while these phenomena were hardly observed in HA-EDA and the nanoconjugate group. Thus it could be concluded that nanoscale conjugates would produce much less injection irritation than cisplatin.

3.12. Hematological parameters and histological analyses

During the clinical practice, major side effects of platinum drugs stem from their serious nephrotoxicity. After successive chemotherapy, concentrations of biomarkers in plasma were determined (Table 1). It's well-known that these parameters are associated with the function of liver (ALT, AST, ALP) and kidney (BUN, Scr) for mammals [19]. Mice treated with the nanomedicine exhibited no significant change of clinical parameters in comparison to control group, denoting negligible systemic toxicity. Unfortunately, mice receiving cisplatin displayed higher levels of all the parameters than physiological saline group, especially BUN and Scr, suggesting high systemic toxicity. On the basis of above observation, greater improvement in reducing side effects was verified in the polymer-drug conjugate group versus cisplatin group.

Table 1 Change of ALT, AST, ALP activities and alteration of BUN, Scr levels in ICR mice plasma.

Group	ALT (IU/L)	AST (IU/L)	ALP (IU/L)	BUN (mmol/L)	Scr (μmol/L)
Physiological saline	39.67 ± 2.52	100.67 ± 2.52	114.67 ± 5.51	6.20 ± 0.95	11.67 ± 2.08

Cisplatin	$81.33 \pm 6.51^{***}$	$198.33 \pm 6.03^{***}$	$180.67 \pm 5.13^{***}$	$18.27 \pm 2.40^{***}$	$24.67 \pm 2.52^{***}$
HA-EDA-Pt(IV) nanoconjugate	$49.33 \pm 2.08^{**\#\#\#}$	$127.33 \pm 5.03^{***\#\#\#}$	$115.67 \pm 2.52^{\#\#\#}$	$4.97 \pm 0.99^{\#\#\#}$	$13.67 \pm 1.53^{\#\#\#}$

422 * Indicates a statistically significant difference compared to physiological saline (*, $p < 0.05$; **, p
423 < 0.01; ***, $p < 0.001$), while $^{\#}$ indicates a statistically significant difference compared to cisplatin
424 ($^{\#}$, $p < 0.05$; $^{\#\#}$, $p < 0.01$; $^{\#\#\#}$, $p < 0.001$).

425

426 Histopathological examination of major organs was shown in Fig. 9(3). It was proved that no
427 significant morphological alternation of heart, spleen, lung and brain was occurred in all groups.
428 Micrographs revealed that hepatocyte injury was negligible in polymer-drug conjugates group,
429 while structural disturbance with vacuolar degeneration of hepatocytes induced by free cisplatin
430 was captured. Moreover, a number of inflammatory cells (mainly neutrophile granulocyte) were
431 infiltrating the renal interstitium only in cisplatin group, which was in agreement with the
432 hematological parameters.

433 Low side effect and great therapeutic effect are always contradictory in cisplatin-based
434 chemotherapy. Multiple-dosed patients usually suffered severe liver and kidney disruption.
435 However, based on strategies of tumor targeted delivery and stimulus-specific drug release and
436 activation, our polymer-drug conjugate was proven safe enough for multiple dose administration,
437 even at a high dose.

438

439 **4. Conclusion**

440 In summary, an anticancer polymer-drug conjugate was prepared by coupling Pt(IV) to HA
441 derivatives. Due to its desirable physicochemical properties as well as advantageous *in vitro* and *in*

vivo behaviors, the nanoconjugate was more likely to extravasate from neo-vasculature to tumors, promote transport via HA receptor-mediated endocytosis, trigger apoptotic signals, and ultimately activate programmed cell death. On the premise of reliable efficacy, safety became a major concern for *in vivo* application. Fortunately, HA-EDA-Pt(IV) nanoconjugate showed negligible peripheral vascular injury and favorable hemocompatibility. In addition, systemic toxicity of cisplatin, especially kidney and liver toxicity, was greatly diminished. Thus, this concise polymer-drug system may improve the therapeutic compliance and advance the clinical application of platinum drugs.

Acknowledgements

This research was supported by the National Natural Science Foundation of China for Young Scholar (NO. 81201182), the Natural Science Foundation of Jiangsu Province for Young Scholar (NO. SBK2015042355), the Fundamental Research Funds for the Central Universities for Cultivation Project (NO. JKPZ2013006) and the Doctoral Fund of Ministry of Education of China for Youth Scholars (NO. 20130096120003).

References

1. Y. Wen and J. H. Collier, *Current Opinion in Immunology*, 2015, **35**, 73-79.
2. C. Engman, Y. Wen, W. S. Meng, R. Bottino, M. Trucco and N. Giannoukakis, *Clinical Immunology*, 2015, **160**, 103-123.
3. A. Balducci, Y. Wen, Y. Zhang, B. M. Helfer, T. K. Hitchens, W. S. Meng, A. K. Wesa and J. M. Janjic, *Oncoimmunology*, 2013, **2**, e23034.
4. Y. Wang, K. Zhou, G. Huang, C. Hensley, X. Huang, X. Ma, T. Zhao, B. D. Sumer, R. J. DeBerardinis and J. Gao, *Nat Mater*, 2014, **13**, 204-212.
5. J. Kreuter, *Advanced Drug Delivery Reviews*, 2014, **71**, 2-14.
6. Y. H. Bae and K. Park, *Journal of Controlled Release*, 2011, **153**, 198.
7. H. Maeda, G. Bharate and J. Daruwalla, *European Journal of Pharmaceutics and*

Biopharmaceutics, 2009, **71**, 409-419.

8. B. R. Schroeder, M. I. Ghare, C. Bhattacharya, R. Paul, Z. Yu, P. A. Zaleski, T. C. Bozeman, M. J. Rishel and S. M. Hecht, *Journal of the American Chemical Society*, 2014, **136**, 13641-13656.

9. Y. Wen, H. R. Kolonich, K. M. Kruszewski, N. Giannoukakis, E. S. Gawalt and W. S. Meng, *Molecular pharmaceutics*, 2013, **10**, 1035-1044.

10. Z. Yu, R. M. Schmaltz, T. C. Bozeman, R. Paul, M. J. Rishel, K. S. Tsosie and S. M. Hecht, *Journal of the American Chemical Society*, 2013, **135**, 2883-2886.

11. Y. Zheng, Y. Wen, A. M. George, A. M. Steinbach, B. E. Phillips, N. Giannoukakis, E. S. Gawalt and W. S. Meng, *Biomaterials*, 2011, **32**, 249-257.

12. C. Li, C. Sun, S. Li, P. Han, H. Sun, A. Ouahab, Y. Shen, Y. Xu, Y. Xiong and J. Tu, *International journal of nanomedicine*, 2014, **9**, 2089-2100.

13. C. Li, S. Li, T. Tu, X. Qi, Y. Xiong, S. Du, Y. Shen, J. Tu and C. Sun, *Polymer Chemistry*, 2015, **6**, 2740-2751.

14. B. Rosenberg, L. Van Camp and T. Krigas, *Nature*, 1965, **205**, 698-699.

15. Y. Xiong, W. Jiang, Y. Shen, H. Li, C. Sun, A. Ouahab and J. Tu, *Biomaterials*, 2012, **33**, 7182-7193.

16. C. Sun, W. C. Shen, J. Tu and J. L. Zaro, *Molecular pharmaceutics*, 2014, **11**, 1583-1590.

17. K. Y. Choi, G. Saravanakumar, J. H. Park and K. Park, *Colloids and Surfaces B: Biointerfaces*, 2012, **99**, 82-94.

18. H. Xiao, R. Qi, S. Liu, X. Hu, T. Duan, Y. Zheng, Y. Huang and X. Jing, *Biomaterials*, 2011, **32**, 7732-7739.

19. H. Xiao, H. Song, Y. Zhang, R. Qi, R. Wang, Z. Xie, Y. Huang, Y. Li, Y. Wu and X. Jing, *Biomaterials*, 2012, **33**, 8657-8669.

20. M. D. Hall, H. R. Mellor, R. Callaghan and T. W. Hambley, *Journal of medicinal chemistry*, 2007, **50**, 3403-3411.

21. Y. Matsumura and H. Maeda, *Cancer research*, 1986, **46**, 6387-6392.

22. S. Aryal, C.-M. J. Hu and L. Zhang, *ACS nano*, 2009, **4**, 251-258.

23. A. Kumar, S. Huo, X. Zhang, J. Liu, A. Tan, S. Li, S. Jin, X. Xue, Y. Zhao and T. Ji, *ACS nano*, 2014, **8**, 4205-4220.

24. V. M. Platt and F. C. Szoka Jr, *Molecular pharmaceutics*, 2008, **5**, 474-486.

25. Y. Shen, B. Wang, Y. Lu, A. Ouahab, Q. Li and J. Tu, *International journal of pharmaceutics*, 2011, **414**, 233-243.

26. X. Ling, Y. Shen, R. Sun, M. Zhang, C. Li, J. Mao, J. Xing, C. Sun and J. Tu, *Polymer Chemistry*, 2015, **6**, 1541-1552.

27. H. T. Duong, V. T. Huynh, P. de Souza and M. H. Stenzel, *Biomacromolecules*, 2010, **11**, 2290-2299.

28. B. Howell, P. Chhetri, A. Dumitrascu and K. Stanton, *Journal of thermal analysis and calorimetry*, 2010, **102**, 499-503.

29. Y. Cho, H. Kim and Y. Choi, *Chemical Communications*, 2013, **49**, 1202-1204.

30. L. Yang, C. F. Fitie, K. O. van der Werf, M. L. Bennink, P. J. Dijkstra and J. Feijen, *Biomaterials*, 2008, **29**, 955-962.

31. Y. Wen, S. L. Roudebush, G. A. Buckholtz, T. R. Goehring, N. Giannoukakis, E. S. Gawalt and W. S. Meng, *Biomaterials*, 2014, **35**, 5196-5205.

32. R. O'leary and W. Guess, *Journal of pharmaceutical sciences*, 1968, **57**, 12-17.

33. M. Reithofer, M. Galanski, A. Roller and B. K. Keppler, *European journal of inorganic chemistry*, 2006, **2006**, 2612-2617.
34. J. Ruan, J. Liu, D. Zhu, T. Gong, F. Yang, X. Hao and Z. Zhang, *International journal of pharmaceutics*, 2010, **386**, 282-290.
35. F. Kagan, M. A. Rebenstorf and R. V. Heinzelman, *Journal of the American Chemical Society*, 1957, **79**, 3541-3544.
36. M. Bujak, L. Sikorska and J. Zaleski, *Zeitschrift für anorganische und allgemeine Chemie*, 2000, **626**, 2535-2542.
37. Y. Wen and W. S. Meng, *Journal of pharmaceutical innovation*, 2014, **9**, 158-173.
38. E. S. Alnemri, D. J. Livingston, D. W. Nicholson, G. Salvesen, N. A. Thornberry, W. W. Wong and J. Yuan, *Cell*, 1996, **87**, 171.
39. D. A. Vezzu, Q. Lu, Y.-H. Chen and S. Huo, *Journal of inorganic biochemistry*, 2014, **134**, 49-56.
40. D. W. Koh, T. M. Dawson and V. L. Dawson, *Pharmacological research*, 2005, **52**, 5-14.
41. D. A. Carson and A. Lois, *The Lancet*, 1995, **346**, 1009-1011.

529 Captions:

530 Fig. 1. Synthesis of (1) Pt(IV); (2) HA-EDA; (3) HA-EDA-Pt(IV) nanoconjugate.

531

532 Fig. 2. ^{1}H NMR spectra of (A) cis,cis,trans-[$Pt(NH_3)_2Cl_2(OH)_2$], (B) Pt(IV) in DMSO-d_6; (C) HA,

533 (D) HA-EDA, (E) HA-EDA-Pt(IV) nanoconjugate in D_2O.

534

535 Fig. 3. ^{13}C NMR spectra of (A) Pt(IV) in DMSO-d_6; (B) HA, (C) HA-EDA, (D) HA-EDA-Pt(IV)

536 nanoconjugate in D_2O.

537

538 Fig. 4. FT-NIR spectra of (A) cisplatin, (B) cis,cis,trans-[$Pt(NH_3)_2Cl_2(OH)_2$], (C) Pt(IV), (D) HA,

539 (E) HA-EDA, (F) HA-EDA-Pt(IV) nanoconjugate.

540

541 Fig. 5. DSC spectra of (A) HA, (B) EDA·2HCl, (C) Pt(IV), (D) the physical mixture of HA,

542 EDA·2HCl and Pt(IV), (E) HA-EDA-Pt(IV) nanoconjugate.

543

544 Fig. 6. (A) Particle size and (B) zeta potential distribution profiles. (C) AFM 3D image and (D)

545 height images of HA-EDA-Pt(IV) nanoconjugate at an optimal dilution ratio.

546

547 Fig. 7. (1) *In vitro* cytotoxicity of HA, HA-EDA, HA-EDA-Pt(IV) nanoconjugate and

548 cisplatin against B16-F10 and Hep G2 at 24 and 48 h. (2) Cellular uptake captured by IFM.

549 Cells were incubated with (A, B) 5 and (C, D) 50 mg/L HA-EDA-Pt(IV)-TRITC (red), (B, D)

550 excessive HA before adding HA-EDA-Pt(IV)-TRITC. Nuclei were stained by DAPI (blue).

551

552 Fig. 8. Activation of (A) Caspase 3, (B) PARP and (C) Phospho-p53 in B16-F10 tumor-bearing
553 mice treated with (a) physiological saline, (b) cisplatin (6 mg/kg), (c) HA-EDA, (d)
554 HA-EDA-Pt(IV) nanoconjugate (6 mg/kg on cisplatin basis). β-actin was probed as a loading
555 control. (D) Quantification of Caspase, PARP, Cleaved PARP and Phospho-p53. The results are
556 the means ± SD from six independent samples.

557

558 Fig. 9. (1) Hemolysis rates of HA, HA-EDA, HA-EDA-Pt(IV) nanoconjugate and Tween 80. (2)
559 Histopathological examination of rabbit ear-rim auricular veins following different injections: (A)
560 physiological saline; (B) HA-EDA; (C) HA-EDA-Pt(IV) nanoconjugate; (D) cisplatin. (3)
561 Histological assessment of major organs (A) physiological saline, (B) cisplatin; (C)
562 HA-EDA-Pt(IV) nanoconjugate.

563

Fig. 1

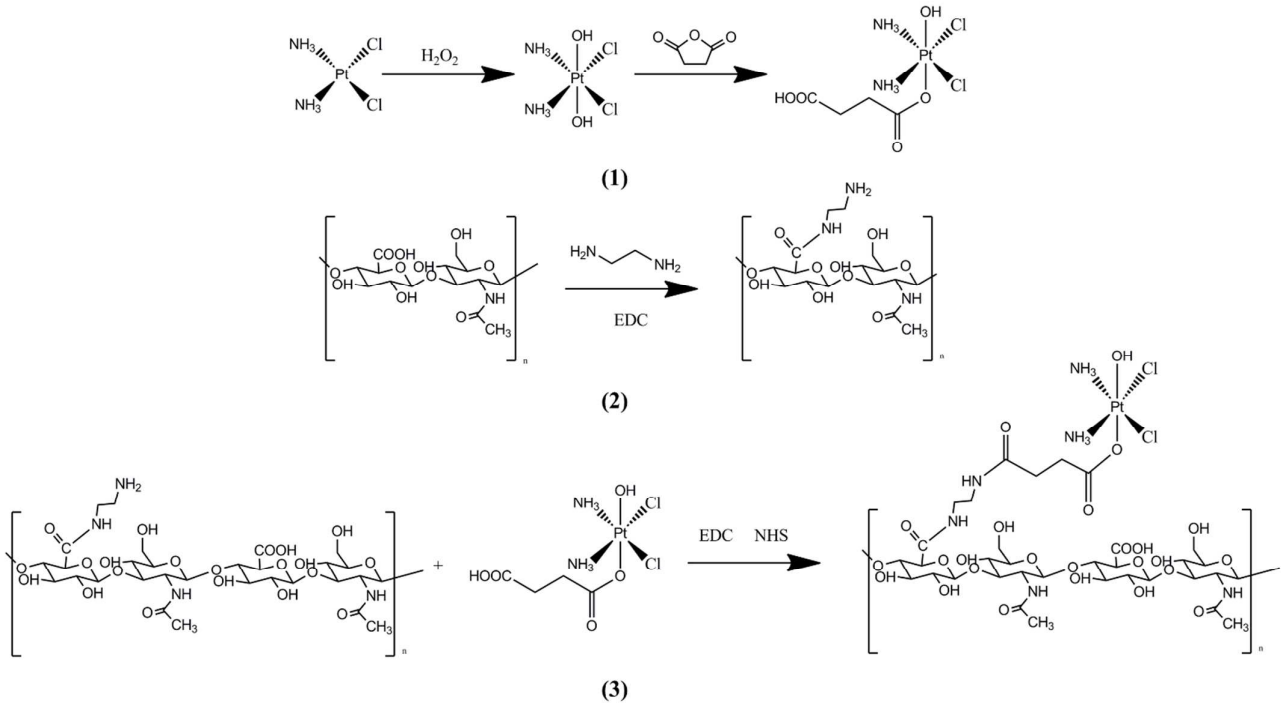

(1)

(2)

(3)

Fig. 2

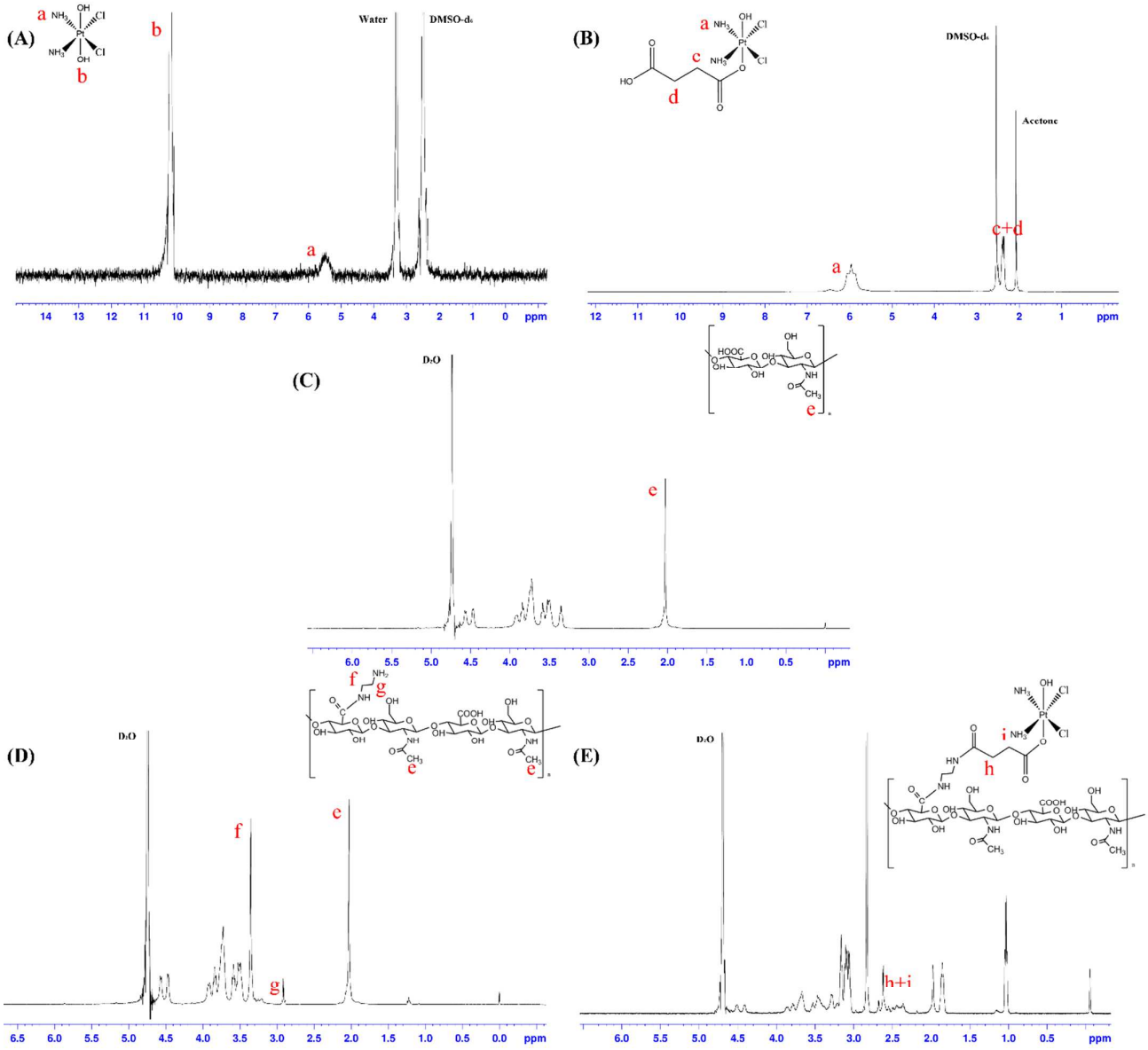

Fig. 3

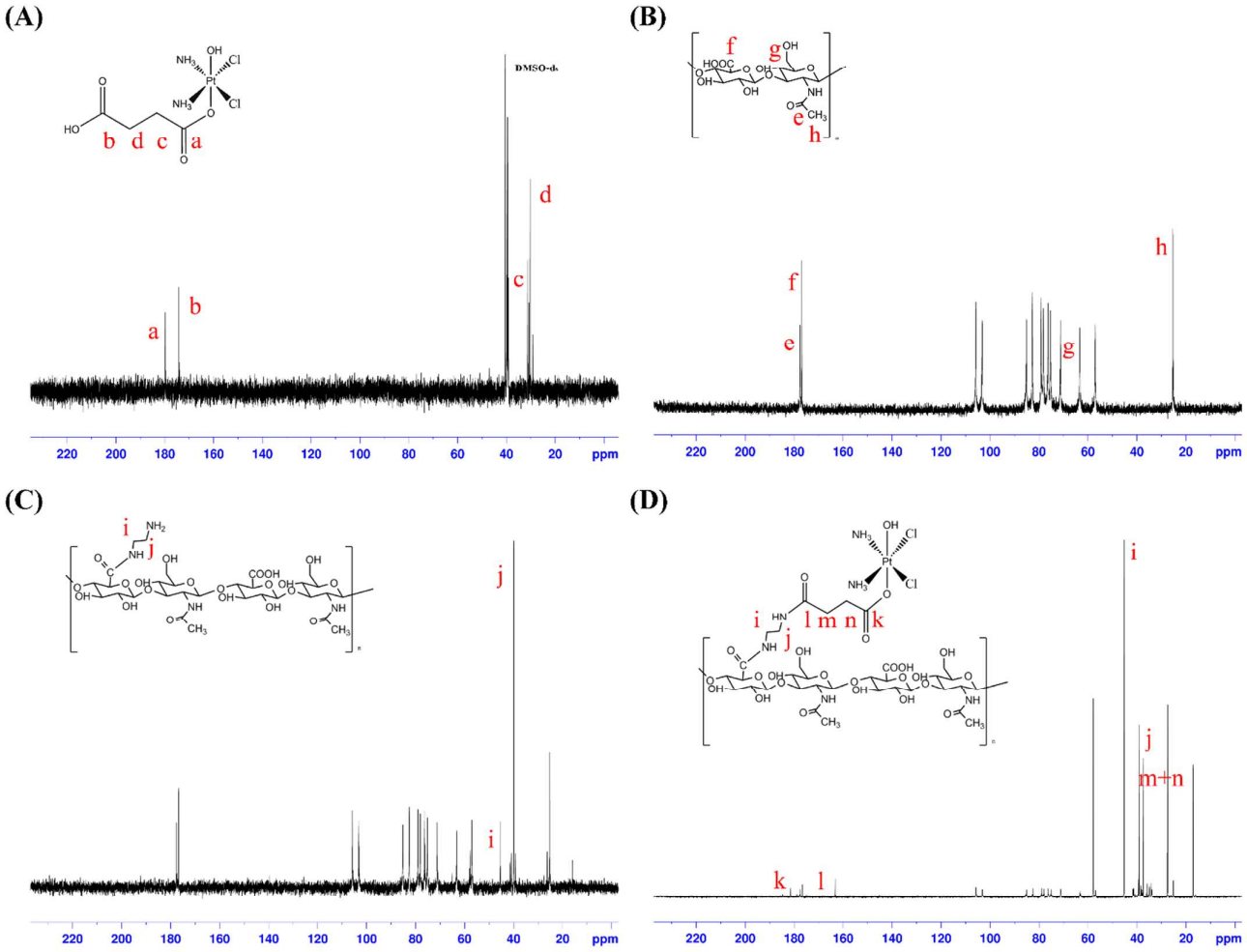

Fig. 4

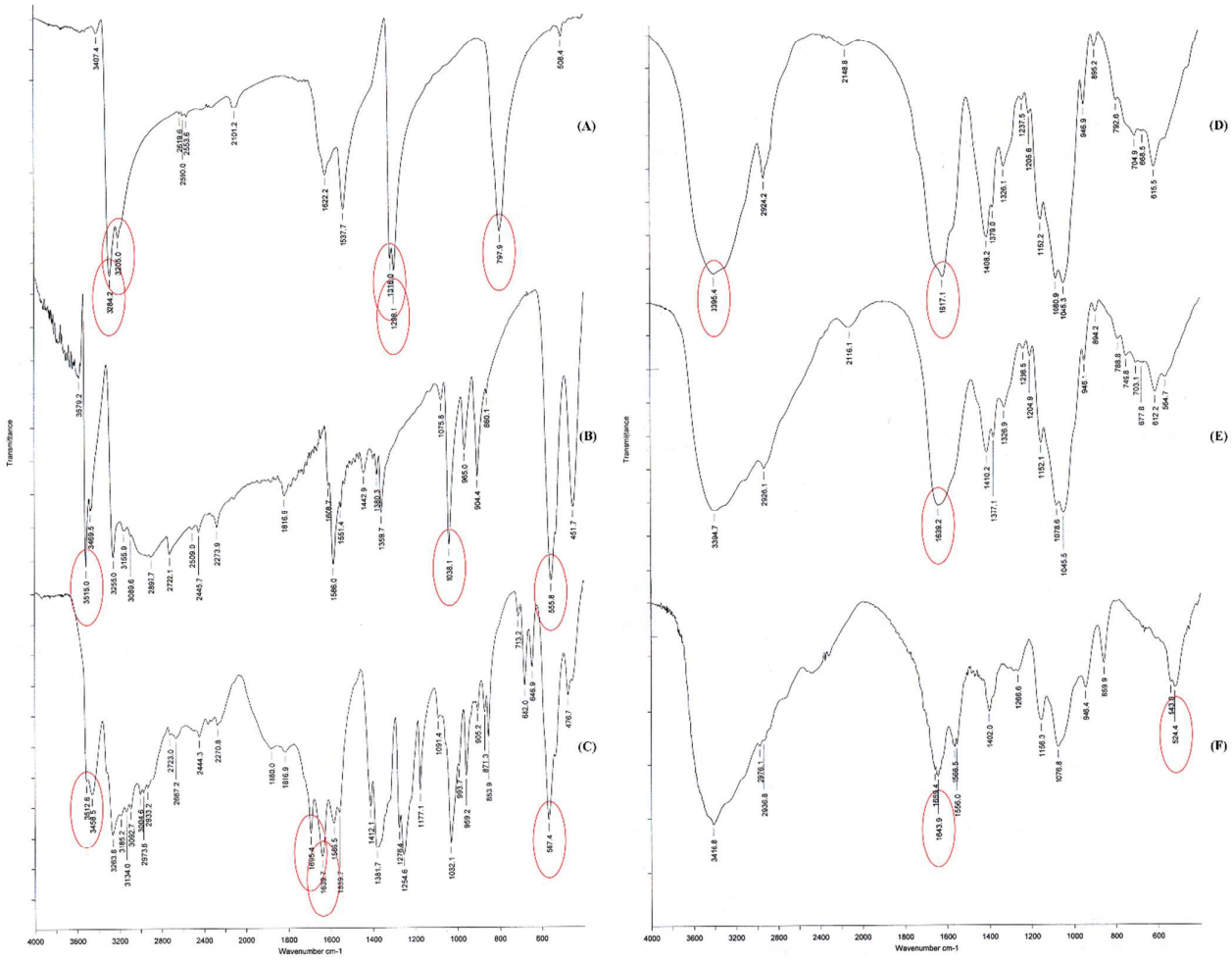

Fig. 5

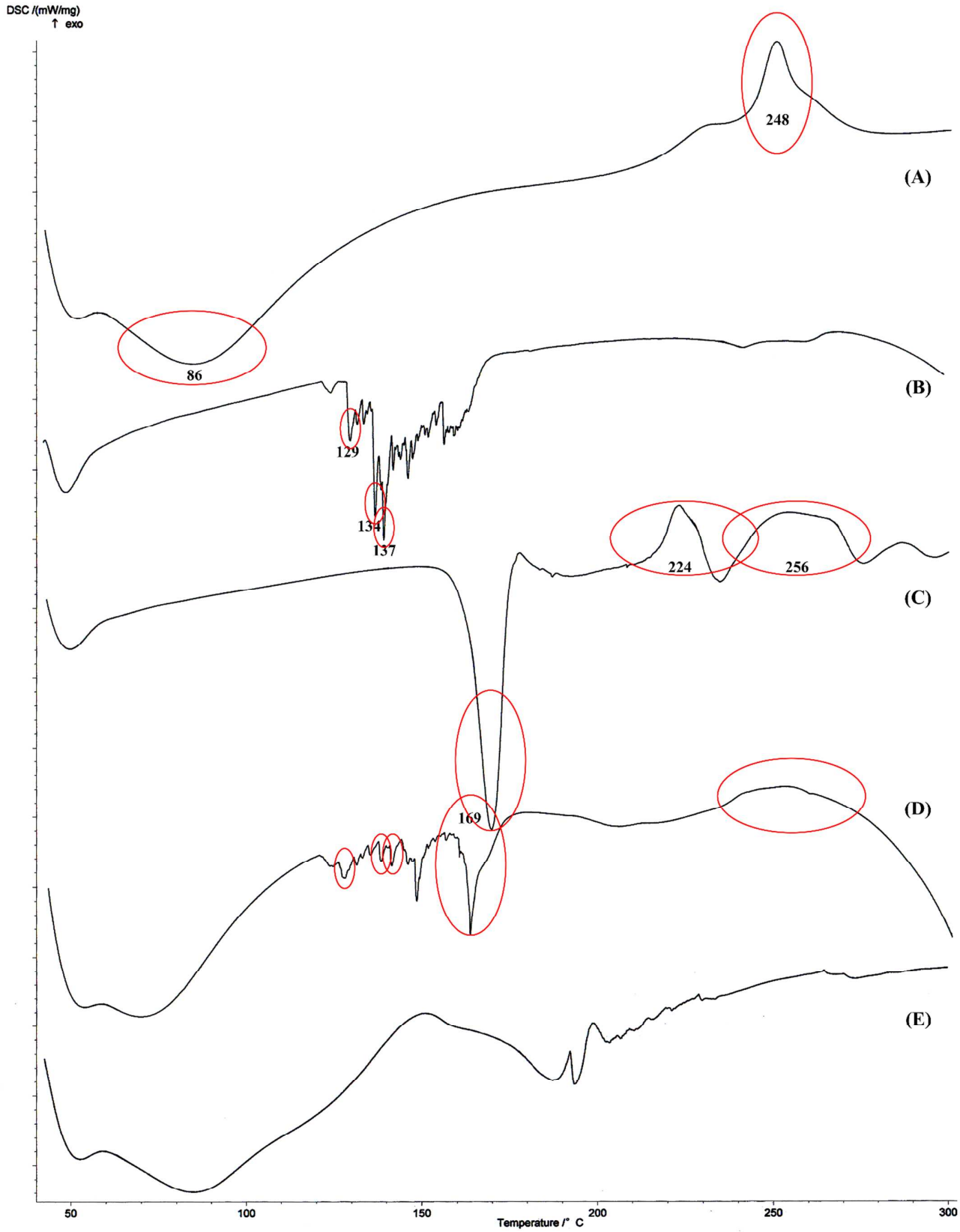

Fig. 6

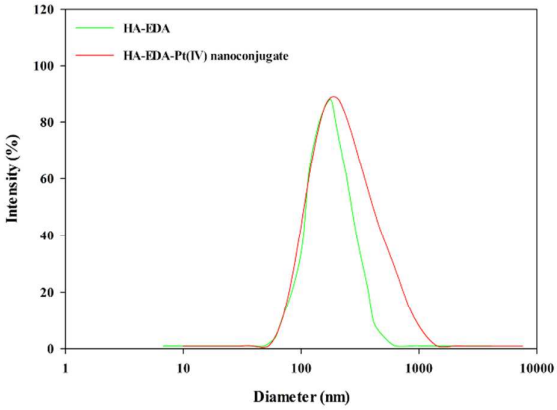

(A)

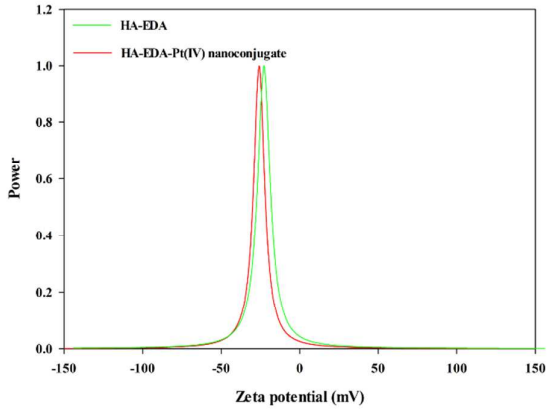

(B)

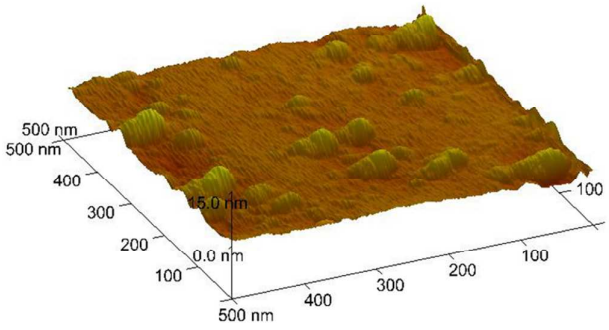

(C)

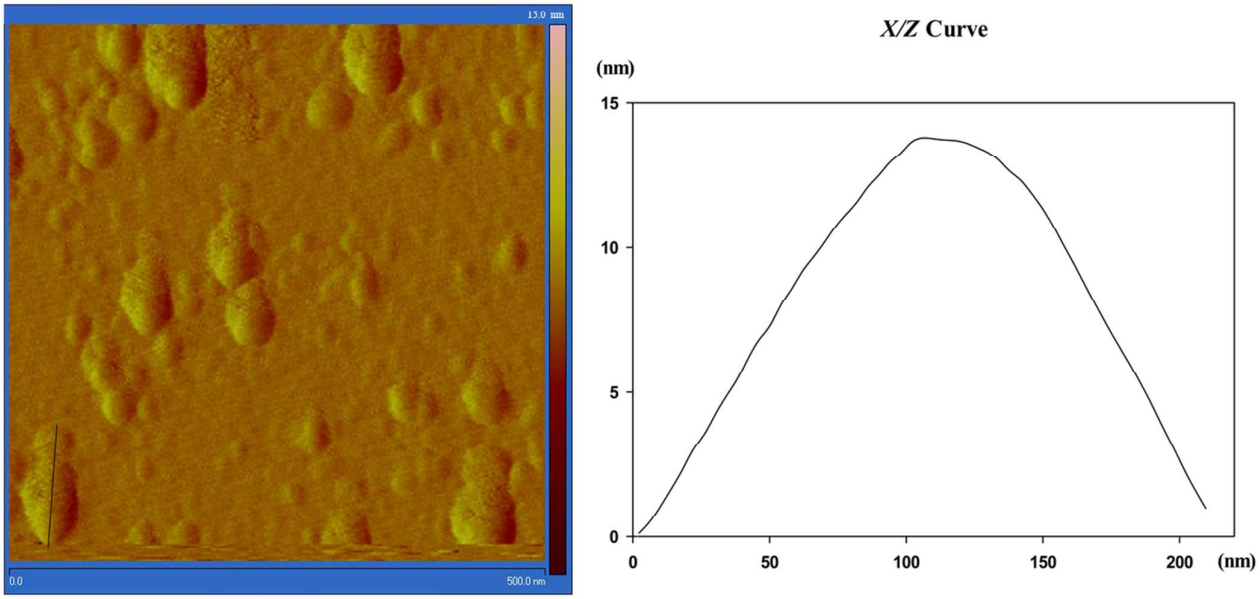

(D)

Fig. 7

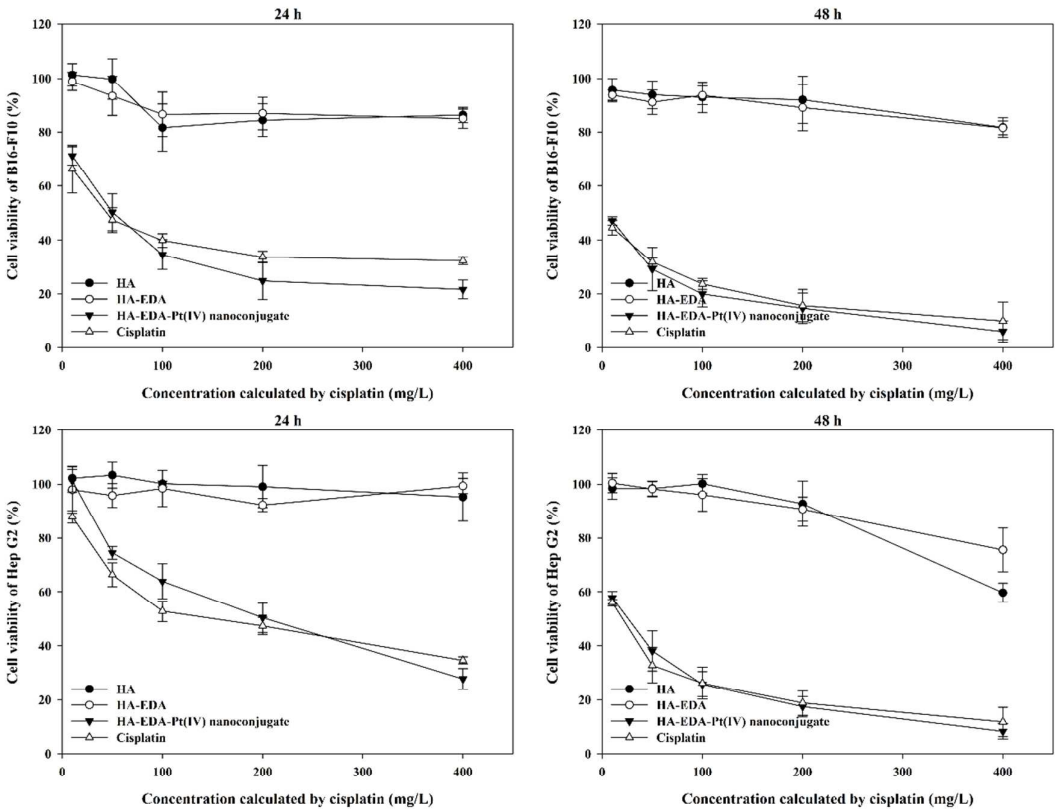

(1)

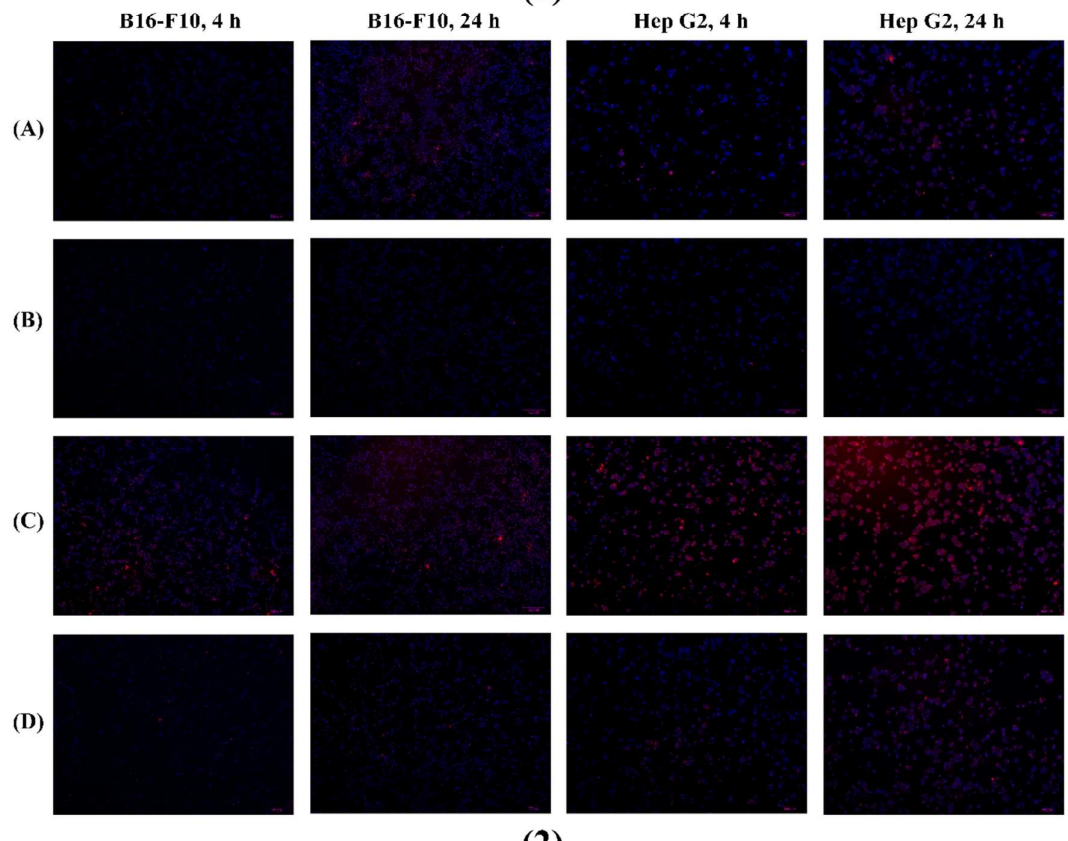

(2)

Fig. 8

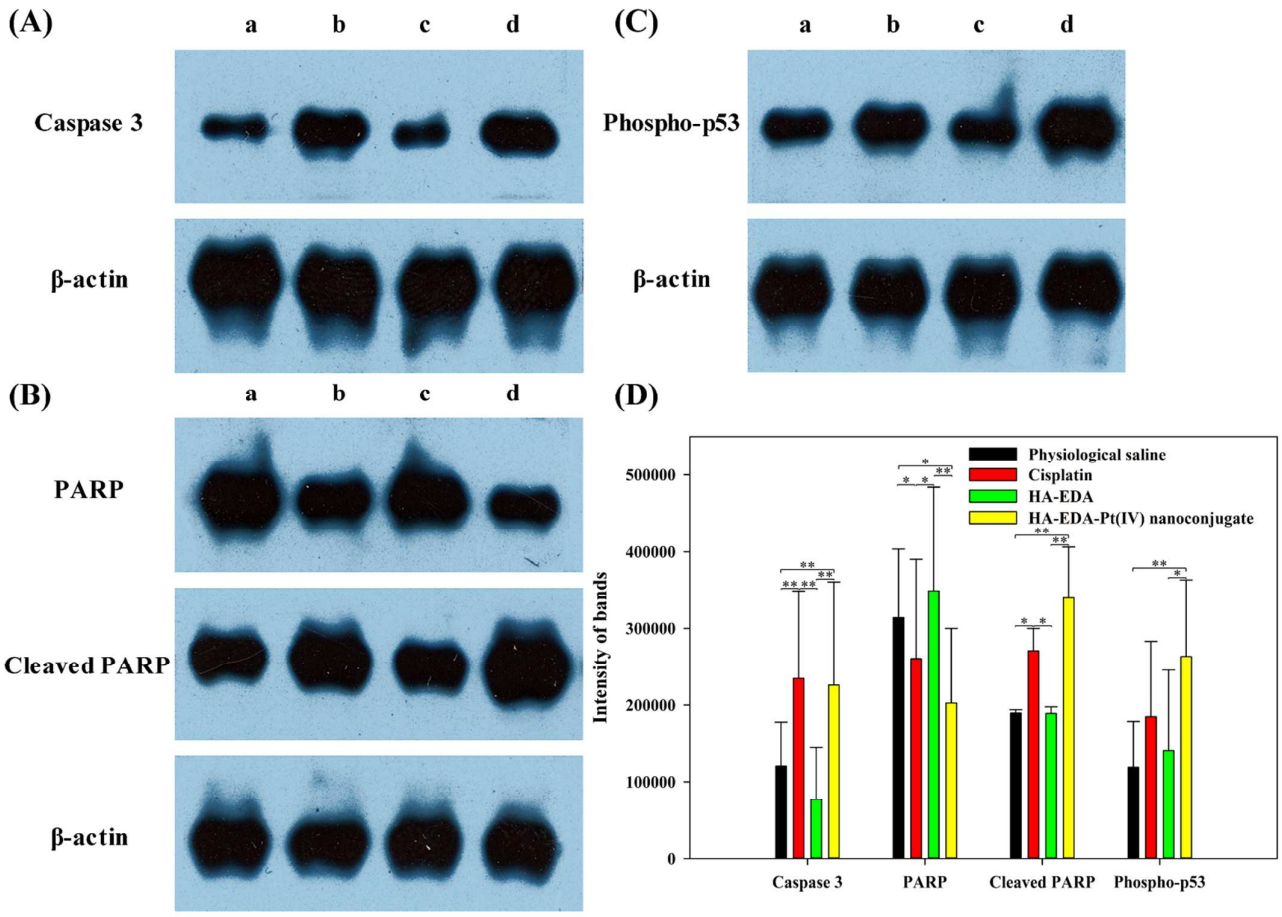

Fig. 9

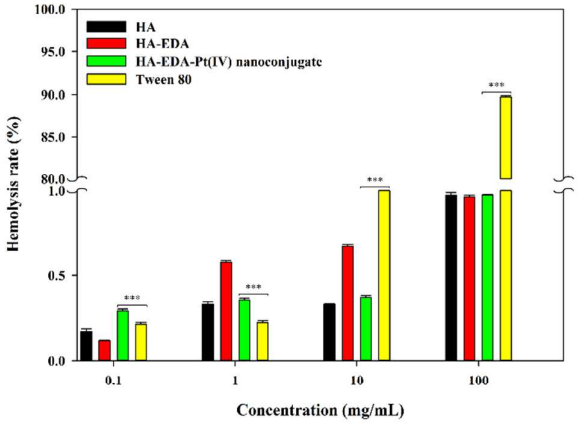

(1)

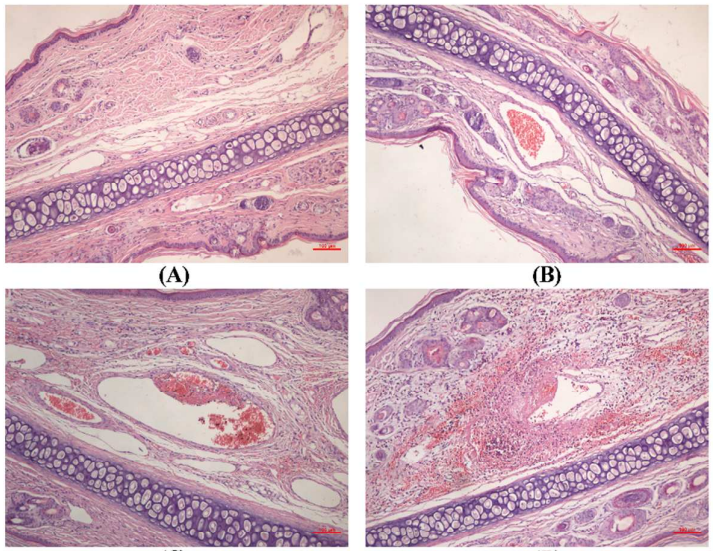

(2)

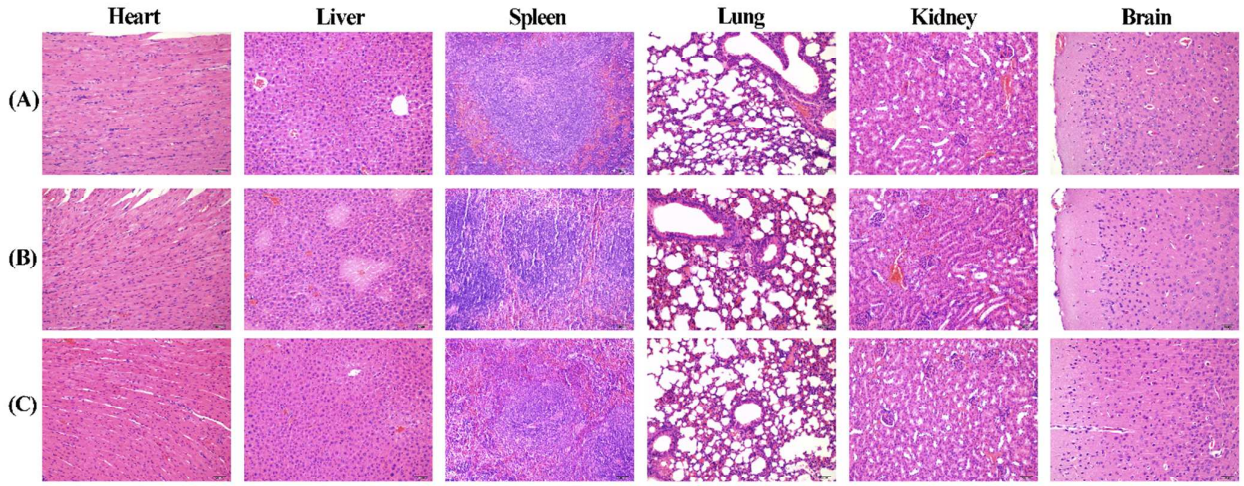

(3)